Preprint

Not Every Breakdown Is Quantum: A Singular-Perturbation Benchmark for Landau–Lifshitz Reduction of Order

Heah Hung Xun, Xu Ya-Xuan

Department of Physics, Xiamen University Malaysia, Sepang, Selangor, Malaysia

E-mail: PHY2409025@xmu.edu.my, PHY2409015@xmu.edu.my

Abstract: The Abraham–Lorentz equation is a singular perturbation: the radiation-reaction time multiplies the highest derivative, and setting it to zero removes the runaway mode by changing the order of the equation. The Landau–Lifshitz equation instead approximates the selected non-runaway branch by a local reduction of order. We quantify this distinction for a nonrelativistic electron driven by a spatially uniform Gaussian electric pulse. The non-runaway acceleration is a future-weighted integral of the force. Parseval's identity then gives an exact finite-ϵ expression for the normalized root-mean-square Landau–Lifshitz error, where $\epsilon = \tau_e/T$. Its small-ϵ expansion is $D_{\mathrm{rms}} = (\sqrt{3}/2)\epsilon^2[1 - \epsilon^2 + O(\epsilon^4)]$; the maximum error is likewise quadratic for the Gaussian pulse. Independent time-domain quadrature reproduces the spectral formula and the asymptotic coefficient. A diagnostic (ϵ, χ_e) map then separates this classical truncation error from quantum-recoil effects governed by χ_e. The result is an exactly checkable benchmark, not a relativistic strong-field prediction: it assumes prescribed one-dimensional motion and the classical point-particle model.

Keywords: Radiation reaction; singular perturbation; reduction of order; Gaussian benchmark; strong-field QED

1 Introduction

Radiation reaction is a basic but subtle problem in classical electrodynamics. An accelerating charge radiates energy and momentum, so a complete equation of motion must include the recoil of the charge on its own field. Imposing energy–momentum conservation on a radiating point charge leads to the Lorentz–Abraham–Dirac (LAD) equation, the covariant point-particle form of this idea. However, LAD is difficult to use directly: it is third order in time and admits runaway solutions whose acceleration grows without bound even after the external force is switched off [1, 3]. The Landau–Lifshitz (LL) equation removes this pathology by reducing the order of LAD and replacing the self-force with a perturbative expression built from the external field and the Lorentz-force motion [2, 5]. For this reason, LL is the form most commonly used in practical calculations.

The difficulty is that the phrase "LL breaks down" can refer to two different questions. The first is a classical approximation question: does LL still track the physical, non-runaway branch of the LAD equation? The second is a physical-validity question: can any deterministic classical equation describe radiation reaction once photon recoil and the stochastic character of emission become important? Strong-field laser physics often couples these two questions, but it does not make them identical. The quantum nonlinearity parameter

$$\chi_{\mathrm{e}} \simeq \frac{\gamma E_{\mathrm{eff}}}{E_{\mathrm{S}}},$$

where γ is the electron Lorentz factor and E_{eff} is the external field it experiences, compares the electron rest-frame field with the Schwinger field E_{S}. It is the standard marker for the onset of quantum emission effects [4]. Recent high-intensity experiments are therefore interpreted through classical, quantum-continuous, and quantum-stochastic models of radiation reaction. The collision experiments of Cole et al. and Poder et al. reported signatures of radiation reaction consistent with quantum descriptions [12, 13], and a recent measurement reports a high-significance observation favouring quantum models over the classical one in the strong-field regime [14]. This vocabulary makes it tempting to identify large χ_{e} with the failure of LL itself. The present paper argues that this identification hides a simpler, purely classical issue underneath the quantum one.

This paper separates the two notions of breakdown in the simplest setting where the LAD–LL comparison can be written explicitly: the nonrelativistic one-dimensional Abraham–Lorentz limit of LAD, for an electron driven by a spatially uniform Gaussian electric pulse. This is a singular-perturbation problem because the radiation-reaction time multiplies the highest derivative and the differential order drops when that time is set to zero. After the non-runaway branch is selected, its acceleration is a future-weighted integral of the applied force, while the LL acceleration is its first local reduction-of-order approximation. The comparison depends on a single dimensionless ratio, the pulse-variation parameter

$$\epsilon = \frac{\tau_{\mathrm{e}}}{T},$$

with τ_{e} the electron radiation-reaction time and T the characteristic pulse duration.

The research question is therefore the following. In the one-dimensional, nonrelativistic Abraham–Lorentz limit for an electron driven by a smooth Gaussian electric pulse, how does the LL approximation deviate from the exact non-runaway acceleration as a function of $\epsilon = \tau_{\mathrm{e}}/T$? How

should that classical accuracy criterion be placed alongside χ_e without confusing reduction-of-order error with quantum radiation-reaction onset?

The claim attached to this question is deliberately modest. This paper proposes no new equation of motion and does not attempt a strong-field QED calculation. Earlier pedagogical work has already compared Abraham–Lorentz and Landau–Lifshitz dynamics, including Gaussian force profiles [6, 7]. The present contribution is an exact normalized L^2 benchmark: a Fourier-space calculation gives $D_{\mathrm{rms}}(\epsilon)$ for every $\epsilon > 0$, its expansion yields $D_{\mathrm{rms}}/\epsilon^2 \to \sqrt{3}/2$ and higher corrections, and independent quadrature checks the result. A diagnostic map then separates the classical parameter ϵ from χ_e without claiming that they are independent in a relativistic experiment.

The distinction is not merely a matter of terminology. Particle-in-cell and single-particle codes used to model laser–plasma interaction and next-generation accelerator stages must choose between a classical radiation-reaction force, a reduced-order equation such as LL, and a stochastic quantum-emission module. This choice is often justified by quoting a value of χ_e [4, 5]. Separating the reduction-of-order error from the quantum-validity question clarifies which choice a given parameter regime actually supports, and which question remains open. The work is best read as a reproducible mathematical-physics benchmark: it supplies a small, exactly checkable test problem for a modelling distinction that appears in larger strong-field codes.

This separation also fixes the scope of the paper. Because the exact non-runaway acceleration is available in closed integral form, the mathematical core remains fully classical and analytically controlled. The strong-field material enters only as interpretation, not as technical overhead. The treatment is nonrelativistic, one-dimensional, and driven by an externally prescribed field; large values of ϵ are used as a controlled diagnostic of the approximation, not as a claim about realistic laboratory pulses, since $\tau_e \sim 6 \times 10^{-24}$ s makes $\epsilon \sim 1$ physically extreme. The project therefore remains within the scope of an undergraduate electrodynamics paper while still connecting to the contemporary literature, where LL, LAD, and quantum-emission models are often compared in the same experimental setting.

The paper is organized as follows. Section 2 reviews the LAD equation, its physical non-runaway branch, and the LL reduction of order. Section 3 constructs the exact non-runaway benchmark in the one-dimensional Abraham–Lorentz limit. Section 4 derives the expected LL error scaling. Section 5 applies the comparison to a Gaussian pulse and reports a compact numerical illustration. Section 6 then interprets the result in relation to χ_e and strong-field radiation reaction.

2 Classical radiation-reaction background

This section fixes the three objects compared in the rest of the paper: the LAD equation, the physical non-runaway branch selected from its solutions, and the LL equation understood as a reduction of order. The aim is to make precise what "LL approximates LAD" means before introducing any pulse shape or numerical calculation. None of this background is new; it is included so that the toy model in Section 3 measures the correct object.

2.1 The LAD equation and its pathologies

In covariant notation, with four-velocity u^μ, proper time τ, and metric signature $(+---)$, the LAD equation can be written schematically as

$$m\frac{\mathrm{d}u^\mu}{\mathrm{d}\tau} = eF^{\mu\nu}u_\nu + m\tau_\mathrm{e}\left(\frac{\mathrm{d}^2u^\mu}{\mathrm{d}\tau^2} + \frac{1}{c^2}\frac{\mathrm{d}u^\alpha}{\mathrm{d}\tau}\frac{\mathrm{d}u_\alpha}{\mathrm{d}\tau}\,u^\mu\right), \tag{2.1}$$

where the radiation-reaction coupling is set by the characteristic time

$$\tau_\mathrm{e} = \frac{2}{3}\,\frac{e^2}{4\pi\epsilon_0\, mc^3} \simeq 6.26\times10^{-24}\ \mathrm{s} \tag{2.2}$$

for the electron. Numerically, τ_e is the time light takes to cross about two-thirds of the classical electron radius. Its extreme smallness is why the radiation-reaction term is a tiny correction in almost all laboratory situations. The two terms in the bracket play different roles. The quadratic piece, proportional to $(\mathrm{d}u^\alpha/\mathrm{d}\tau)(\mathrm{d}u_\alpha/\mathrm{d}\tau)\,u^\mu$, is the dissipative part: it carries away four-momentum at the relativistic Larmor rate and has the character of radiative friction. The Schott term $\mathrm{d}^2u^\mu/\mathrm{d}\tau^2$ is the source of the mathematical difficulty. Because it contains a second proper-time derivative of the velocity, equation (2.1) is third order in the position. Position and velocity at one instant no longer determine the trajectory; an initial acceleration must also be specified.

This extra initial datum is where the pathology enters. The freedom it represents is a runaway mode: even with $F^{\mu\nu} = 0$, the equation admits self-accelerating histories in which the proper acceleration grows like e^{τ/τ_e} [1, 3, 5]. Generic initial accelerations excite this mode, and the particle accelerates itself to the speed of light with no applied force. These histories are genuine mathematical solutions of the differential equation, but they are not accepted as physical electron motions. A prescription is therefore needed to discard them.

2.2 The physical non-runaway branch

Removing the runaways requires an additional condition. The standard condition, due to Dirac, is imposed in the future rather than the past: the acceleration is required to vanish asymptotically once the external force is switched off. Tuning the initial acceleration to meet this condition selects a distinguished branch of solutions and removes the runaway freedom, at the cost of making the dynamics nonlocal in time. On this branch the acceleration at a given instant depends on the force still to come, and the charge can begin to accelerate slightly before the force arrives, over a window of order τ_e. This pre-acceleration is a property of the selected branch, not a numerical artifact of a particular integration scheme, and at accessible pulse durations it is far too small and too brief to be observed.

Spohn's critical-manifold picture gives this selection a geometric interpretation. The physically admissible solutions lie on a low-dimensional invariant ("critical") manifold in the LAD phase space. Transverse to that manifold, the dynamics is the runaway: off-manifold perturbations grow like e^{τ/τ_e}, so the transverse directions are repelling in forward time. Dirac's asymptotic condition is what restricts the motion to the manifold. The reduced motion on the manifold can then be obtained perturbatively, which is the modern justification for replacing the full third-order system with an effective second-order equation [3]. The same physical branch can be studied by other routes; for

planar motion in a constant field, for instance, the dynamics reduces to a single second-order equation whose large-proper-time asymptotics can be obtained explicitly [17]. The formal structure of the runaway-free reduction, including the way the perturbative series encodes the discarded modes, has also been analysed using transseries [10].

The practical consequence is important for the rest of the paper. The correct benchmark for LL is the physical branch, not arbitrary LAD initial data; comparing LL with a runaway-contaminated solution would test the wrong object. It also means that the benchmark can be built from a stable closed-form representation of the non-runaway solution, as done in Section 3, rather than from an unstable third-order initial-value integration.

2.3 LL as a reduction of order

The full relativistic LL equation replaces the self-force in (2.1) with terms built from derivatives of the external field along the trajectory and from quadratic field combinations [2]. The construction is a reduction of order: one takes the small radiation-reaction term, which carries the troublesome higher derivative, and substitutes into it the lowest-order (Lorentz-force) acceleration, $\mathrm{d}u^\mu/\mathrm{d}\tau \approx (e/m)F^{\mu\nu}u_\nu$. Differentiating that lowest-order relation turns the Schott term into an expression involving the field gradient and the field squared, with no second derivative of the velocity left to supply as initial data. The result is a second-order equation with no runaways, and it is the form normally adopted as the working classical model of radiation reaction [5].

Two cautions follow from this step and shape the present project. First, reduction of order is a perturbative substitution. It is valid when the self-force is a genuinely small correction, so it should be read as a controlled local approximation for smooth fields, not as an exact rewriting of the physical branch. Second, the reduction-of-order expansion is generally asymptotic rather than convergent: LL is its first term, often an optimal low-order truncation, but additional terms need not improve it and can miss short-time, resummed behaviour [9]. Both cautions are easiest to see in the simplest case, where the tensor structure of (2.1) collapses and the substitution can be carried out by hand. In the nonrelativistic one-dimensional limit, the radiation-reaction term $\tau_\mathrm{e}\,\dot{a}$ has the lowest-order acceleration $a \approx F/m$ inserted into it, giving the local approximation $a_\mathrm{LL} = F/m + \tau_\mathrm{e}\dot{F}/m$. The next section therefore specializes to this Abraham–Lorentz limit, in which the physical branch is an elementary integral and LL is its first derivative correction.

3 Exact non-runaway benchmark in the Abraham–Lorentz limit

3.1 Nonrelativistic reduction

Specializing the covariant equation (2.1) to one spatial dimension and nonrelativistic motion reduces its tensor structure to a single scalar relation. For an electron in a spatially uniform, time-dependent electric field $E(t)$, the Lorentz factor is $\gamma \approx 1$, the magnetic force vanishes, and the dissipative quadratic term in (2.1) is higher order in v/c and drops at leading order. The self-force then keeps only the Schott contribution, and the equation of motion becomes the Abraham–Lorentz form

$$a(t) = \frac{F(t)}{m} + \tau_\mathrm{e}\,\dot{a}(t), \tag{3.1}$$

where $F(t) = -eE(t)$ is the externally prescribed force and $a = \dot{v}$. The field is taken as a function of time alone: spatial gradients are dropped, so the force does not depend on the particle position and the electron does not act back on the field. This is the standard test-charge reading of the problem, and it is the price of solvability; its limits are revisited in Section 6. Equation (3.1) is the nonrelativistic one-dimensional Abraham–Lorentz limit of LAD, and it inherits both difficulties identified in Section 2. It is effectively of higher order, because the self-force depends on $\dot{a}$ rather than on a alone, and its homogeneous solutions run away.

It is also a singularly perturbed equation. The small parameter τ_e multiplies the highest derivative of a, so the limit $\tau_e \to 0$ lowers the differential order and removes an initial datum. A regular expansion of arbitrary solutions cannot capture that change: generic solutions contain the runaway Ce^{t/τ_e}, which is non-analytic at $\tau_e = 0$. Reduction of order becomes meaningful only after the non-runaway branch has been selected. This order loss is the mathematical reason that the Landau–Lifshitz prescription is more than simply "setting a small term to zero."

Setting $F = 0$ in equation (3.1) makes this explicit: the source-free equation $a = \tau_e \dot{a}$ has the solution $a(t) \propto e^{t/\tau_e}$. Every solution of the driven equation is therefore fixed only up to an additive multiple of this runaway mode, so equation (3.1) by itself does not determine the physical motion. Selecting the physical branch requires the supplementary condition discussed in Section 2.2, now applied to the scalar equation: the acceleration must not grow like the runaway mode once the pulse has passed.

3.2 Exact non-runaway solution

Equation (3.1) is a linear first-order equation for $a(t)$. Rearranging it as $\dot{a} - a/\tau_e = -F/(m\tau_e)$ and multiplying by the integrating factor e^{-t/τ_e} gives

$$\frac{\mathrm{d}}{\mathrm{d}t}\left[a(t)\, e^{-t/\tau_e}\right] = -\frac{1}{m\tau_e} F(t)\, e^{-t/\tau_e}. \tag{3.2}$$

The general solution is a particular integral plus a multiple of the homogeneous runaway e^{t/τ_e}. Integrating equation (3.2) from t to ∞ and imposing the non-runaway condition $a(t)\, e^{-t/\tau_e} \to 0$ as $t \to \infty$ removes the boundary term at infinity, fixes the homogeneous coefficient to zero, and yields a unique result,

$$a_{\mathrm{LAD}}(t) = \frac{1}{m\tau_e} \int_t^\infty \exp\left[-\frac{t' - t}{\tau_e}\right] F(t')\, \mathrm{d}t'. \tag{3.3}$$

Equation (3.3) is the exact physical acceleration in this model and the benchmark against which the LL approximation is measured throughout the paper. The substitution $t' = t + \tau_e u$ casts it in the compact form

$$a_{\mathrm{LAD}}(t) = \frac{1}{m} \int_0^\infty e^{-u}\, F(t + \tau_e u)\, \mathrm{d}u, \tag{3.4}$$

which is the representation expanded in Section 4 and evaluated numerically in Section 5.

Equation (3.3) can also be read as a Green-function statement. The operator on the left of equation (3.1), written $1 - \tau_e\, \mathrm{d}/\mathrm{d}t$ acting on a, has a future-decaying inverse whose kernel is $\tau_e^{-1} e^{-(t'-t)/\tau_e}$ for $t' > t$ and zero otherwise. Equation (3.3) is the convolution of that kernel with F/m. Selecting the future-decaying Green function rather than the past-decaying one is the same choice as discarding the runaway mode, now phrased as a boundary condition for an inhomogeneous

linear equation. This is the one-dimensional, nonrelativistic image of the critical-manifold reduction of Section 2.2: the manifold is the single physical solution (3.3), and the discarded transverse direction is the growing exponential.

Two properties of equation (3.3) carry the physics. The acceleration at time t is a weighted average of the force at *later* times $t' > t$, with the exponential kernel $e^{-(t'-t)/\tau_e}$ setting the weight. The electron therefore responds to the force over a forward window of width of order τ_e. This forward weighting is the origin of pre-acceleration and is formally acausal: the particle begins to accelerate before the applied force reaches it. Selecting the non-runaway branch removes one pathology at the price of retaining this one. The effect is confined to the microscopic timescale τ_e, but that smallness does not turn it into a causal solution. The kernel is normalized, $\frac{1}{\tau_e}\int_t^\infty e^{-(t'-t)/\tau_e}\,\mathrm{d}t' = 1$, so a static force returns $a = F/m$ and the ordinary Newtonian result is recovered whenever radiation reaction is negligible.

3.3 Meaning of the benchmark

The usefulness of equation (3.3) is both practical and conceptual. It writes the non-runaway branch as a convergent integral of the applied force, so the physical acceleration can be evaluated by quadrature without integrating the unstable third-order dynamics forward in time. This makes a clean numerical comparison with LL possible, and it is why Section 5 computes equation (3.3) directly rather than solving equation (3.1) as an initial-value problem. The exponential suppression in equation (3.4) also makes the quadrature simple: the integrand decays like e^{-u}, so a modest truncation of the u integral captures the solution to high accuracy.

The construction is exact only within the simplified model: the field is uniform and prescribed, the motion is nonrelativistic and one-dimensional, and the point-particle picture is assumed. Inside those limits the integral is not an approximation but the physical branch itself. This identification is consistent with recent analysis treating LL as the first term of a reduction-of-order series whose higher orders form a divergent, asymptotic expansion, and showing in solvable field configurations that resumming the series reconstructs a runaway-free physical solution rather than a new equation [9]. Equation (3.3) is the nonrelativistic, closed-form instance of that physical branch. It is also the natural object against which to test how short a pulse may be, in units of τ_e, before the first local correction stops being adequate; that question becomes quantitative once the kernel acts on a specific force profile. The next section expands equation (3.4) to recover LL and to identify the leading discrepancy.

4 LL approximation and expected deviation

4.1 Expansion of the physical solution

The compact form (3.4) of the physical acceleration is built for expansion. When the force is smooth and varies slowly on the scale τ_e, the shift $\tau_e u$ inside $F(t + \tau_e u)$ is small over the range where the kernel e^{-u} has support. We can then Taylor-expand F about t,

$$F(t + \tau_e u) = \sum_{n=0}^{\infty} \frac{(\tau_e u)^n}{n!} F^{(n)}(t). \tag{4.1}$$

Inserting equation (4.1) into (3.4) and using the elementary moments of the exponential kernel,

$$\int_0^\infty e^{-u}\, u^n \, \mathrm{d}u = n!, \tag{4.2}$$

makes every term collapse to a single derivative, because the factorials cancel. The result is the local derivative series, to be read as an asymptotic expansion in τ_e (see Section 4.2),

$$a_{\mathrm{LAD}}(t) \sim \frac{1}{m} \sum_{n=0}^{\infty} \tau_e^n F^{(n)}(t) = \frac{1}{m} \left[F(t) + \tau_e \dot{F}(t) + \tau_e^2 \ddot{F}(t) + \cdots \right]. \tag{4.3}$$

Each derivative of the force is accompanied by one extra power of τ_e, so the size of successive terms is controlled by how rapidly F varies relative to τ_e.

4.2 LL as the first local approximation

The nonrelativistic LL acceleration is the truncation of equation (4.3) after the first correction,

$$a_{\mathrm{LL}}(t) = \frac{1}{m} \left[F(t) + \tau_e \dot{F}(t) \right], \tag{4.4}$$

which is exactly the reduction-of-order result obtained in Section 2.3 by substituting the lowest-order acceleration into the radiation-reaction term. Subtracting it from the exact series isolates the leading discrepancy,

$$a_{\mathrm{LAD}}(t) - a_{\mathrm{LL}}(t) = \frac{\tau_e^2}{m} \ddot{F}(t) + O(\tau_e^3). \tag{4.5}$$

If the force varies on a characteristic time scale T, then $F^{(n)} \sim F/T^n$, and the nth term in equation (4.3) is of relative size $(\tau_e/T)^n = \epsilon^n$. The first neglected term is therefore of order ϵ^2, and equation (4.5) predicts a fractional acceleration-level difference scaling as ϵ^2, except near zeros of the force where the denominator vanishes and relative errors become ill-conditioned.

This estimate also explains why the comparison is about time variation rather than force strength. In the linear Abraham–Lorentz benchmark, the amplitude of F multiplies every term in equation (4.3). It therefore cancels from any normalized difference between the physical acceleration and the LL acceleration. What remains is the rate at which the force changes over the short memory time τ_e. A strong but slowly varying field can still be well approximated by LL as a classical reduction of order, while a weak field that changes over a time comparable to τ_e would be a poor case for the first-order truncation. This point is artificial in the sense that realistic optical pulses never approach $T \sim \tau_e$, but it is useful because it isolates the mathematical small parameter of the reduction of order.

The estimate should be read as an error statement for an acceleration profile, not as a statement about total radiated energy alone. Energy loss depends on integrals of the acceleration and can sometimes hide local discrepancies through cancellations. By contrast, the acceleration comparison used here asks a stricter question: at each time, does the local LL rule reproduce the physical non-runaway acceleration selected by the future boundary condition? The answer is yes to first order in ϵ and no at second order, with the leading miss proportional to the curvature of the applied force. For the Gaussian pulse, this places the largest discrepancy near the pulse centre, where the force profile bends most strongly, rather than in the far tails where the force is already negligible.

The expansion must not be read as a proof that adding further reduction-of-order corrections always improves the approximation. The derivative series (4.3) is generally asymptotic rather than convergent: successive terms can grow, and the formal sum need not converge to the physical solution [9, 10]. In the constant-crossed-field case the reduction-of-order series is explicitly divergent, and resumming it reproduces a runaway-free physical solution rather than diverging without meaning [9]. The practical reading is that LL is the first, and often an optimal low-order, truncation. Equation (4.5) is a controlled leading estimate of its error for smooth pulses with $\epsilon \ll 1$, not an exact remainder, and it says nothing reliable about the behaviour of higher truncations.

There is a useful physical picture behind the same algebra. The exact branch in equation (3.4) averages the future force over an exponential window of width τ_e. LL replaces that weighted average by the value of the force now plus its first local slope. If the force is nearly straight over the memory window, this linear replacement is accurate. If the force has appreciable curvature over that window, LL cannot know it, because all information beyond the first derivative has been discarded. The leading curvature term $\tau_e^2 \ddot{F}/m$ is therefore the mathematical trace of the nonlocal information lost when the physical LAD branch is compressed into a local second-order equation. This is why the benchmark uses a smooth pulse: it lets the local expansion fail gradually and measurably, rather than through a discontinuity where the derivative series itself would not be defined.

4.3 Hypotheses for the numerical section

The leading estimate (4.5) turns into three concrete predictions for the Gaussian-pulse comparison in Section 5.

1. A normalized root-mean-square difference between a_{LAD} and a_{LL} should scale approximately as ϵ^2 for $\epsilon \ll 1$, that is, with slope close to 2 on a log–log plot against ϵ.

2. The largest pointwise deviations should appear where $|\ddot{F}|$ is largest, near the pulse peak, and should grow as ϵ approaches unity, where the truncation (4.4) loses control.

3. Changing the field amplitude rescales a_{LAD} and a_{LL} together, so it changes χ_e but leaves the normalized LL–LAD error unchanged in this linear benchmark.

The next section tests all three against a direct numerical evaluation of the exact integral.

5 Gaussian-pulse numerical illustration

5.1 Model and dimensionless variables

The external field is a spatially uniform Gaussian electric pulse,

$$E(t) = E_0 \exp\left(-\frac{t^2}{2T^2}\right), \qquad B = 0, \tag{5.1}$$

acting on an initially nonrelativistic electron, so that $F(t) = -eE(t)$ with peak magnitude $F_0 = eE_0$. The Gaussian is a convenient test profile because it is smooth, has a single time scale T, and

has derivatives of every order, so the expansion of Section 4 applies cleanly. Three dimensionless variables organize the comparison,

$$s = \frac{t}{T}, \qquad \epsilon = \frac{\tau_e}{T}, \qquad \kappa = \frac{E_0}{E_S}. \tag{5.2}$$

Here s is time in units of the pulse duration, ϵ is the reduction-of-order parameter, and κ is the field amplitude in units of the Schwinger field. In the nonrelativistic electric-only limit, the quantum parameter of Section 6 is $\chi_e \simeq \gamma\kappa$. Since the benchmark electron is nonrelativistic ($\gamma \approx 1$), $\chi_e \approx \kappa$ here, and the general $\gamma\kappa$ form is kept for Section 6. Thus κ sets χ_e while ϵ is fixed entirely by the pulse duration. The acceleration is reported in units of F_0/m, with an overall sign absorbed so that the normalized profiles are positive and the error metrics below are sign-independent ratios. In these units the normalized LL–LAD error depends only on ϵ, not on E_0: rescaling the amplitude multiplies a_{LAD} and a_{LL} by the same factor. This is hypothesis 3 of Section 4.3, and it holds by construction in the linear model.

5.2 Numerical method and error metrics

In dimensionless form the exact physical acceleration follows from equation (3.4),

$$\frac{m\, a_{\mathrm{LAD}}(s)}{F_0} = \int_0^\infty e^{-u} \exp\left[-\frac{(s+\epsilon u)^2}{2}\right] \mathrm{d}u, \tag{5.3}$$

and the LL approximation (4.4) becomes

$$\frac{m\, a_{\mathrm{LL}}(s)}{F_0} = \exp\left(-\frac{s^2}{2}\right) - \epsilon\, s \exp\left(-\frac{s^2}{2}\right). \tag{5.4}$$

The two profiles are compared with a relative root-mean-square and a relative maximum metric,

$$D_{\mathrm{rms}} = \left[\frac{\int (a_{\mathrm{LAD}} - a_{\mathrm{LL}})^2 \,\mathrm{d}s}{\int a_{\mathrm{LAD}}^2 \,\mathrm{d}s}\right]^{1/2}, \qquad D_{\max} = \frac{\max_s |a_{\mathrm{LAD}} - a_{\mathrm{LL}}|}{\max_s |a_{\mathrm{LAD}}|}. \tag{5.5}$$

The integral (5.3) is evaluated by composite Simpson quadrature in u. The kernel e^{-u} suppresses the integrand exponentially, so the calculation truncates at $u_{\max} = 40$ and uses 2400 subintervals. The acceleration profiles are sampled on a uniform s grid over $[-10, 10]$ with 2401 points, and the metric integrals in equation (5.5) are evaluated by the trapezoidal rule. The scan runs over $\epsilon \in [0.01, 1.0]$. The full calculation is performed by a dependency-free Python script, so the figures and Table 1 are reproducible from the source provided with this project.

The strongest accuracy check is independent of that time-domain discretization. The script also evaluates the exact frequency-domain identity (5.9); its D_{rms} differs from the future-integral calculation by at most 6.5×10^{-9} across the scan. Doubling the s-grid density in the representative cases $\epsilon = 0.05, 0.5, 1$ changes D_{rms} by at most 1.3×10^{-13} and $D_{\max}$ by at most 1.2×10^{-6}. The one place where care is needed is the definition of the relative error itself. A pointwise ratio $|a_{\mathrm{LAD}} - a_{\mathrm{LL}}|/|a_{\mathrm{LAD}}|$ becomes ill-conditioned in the tails. The metrics in equation (5.5) are therefore integrated or peak-normalized, keeping them finite and dominated by the pulse region.

The numerical calculation is intentionally more transparent than efficient. Since the problem is one-dimensional and the kernel is positive, direct quadrature is clearer than solving the differential

equation as an initial-value problem and then trying to suppress its runaway mode. It also makes the physical boundary condition visible in the code: every value of $a_{\mathrm{LAD}}(s)$ is obtained by averaging future values of the force with the weight e^{-u}. The script therefore implements the same object as the analytic derivation, not a different numerical regularization of LAD. This matters pedagogically, because the goal is to compare LL with the physical branch rather than with a numerically stabilized third-order trajectory.

The scan separates three kinds of evidence. Table 1 tests the scaling law quantitatively, Figure 1 shows the local shape of the discrepancy, and Figure 2 checks whether the same scaling survives across several decades of ϵ. No single one of these is sufficient. A table alone could hide where in the pulse the error occurs; profile plots alone could exaggerate a visually striking but small integrated error; and a log–log plot alone would not fix the numerical coefficient. Taken together they provide a compact consistency check on the analytic argument.

5.3 Results

Table 1 lists the two error metrics over the scanned range, together with the ratio $D_{\mathrm{rms}}/\epsilon^2$. This ratio is the cleanest test of the predicted scaling: if the leading error is $O(\epsilon^2)$, it should approach a constant as $\epsilon \to 0$. It does: the value settles near 0.86 for the smallest pulses and drifts downward only as ϵ grows toward unity, where the higher-order terms dropped by LL begin to matter.

Table 1. Numerical comparison for the Gaussian pulse, from direct quadrature of equation (5.3) with the documented script. The near-constant ratio $D_{\mathrm{rms}}/\epsilon^2$ at small ϵ confirms the predicted leading scaling; its decline at large ϵ marks the onset of higher-order corrections.

$\epsilon = \tau_{\mathrm{e}}/T$	D_{rms}	D_{max}	$D_{\mathrm{rms}}/\epsilon^2$
0.02	3.46×10^{-4}	4.00×10^{-4}	0.866
0.05	2.16×10^{-3}	2.49×10^{-3}	0.864
0.10	8.58×10^{-3}	9.90×10^{-3}	0.858
0.20	3.34×10^{-2}	3.86×10^{-2}	0.835
0.50	1.83×10^{-1}	2.14×10^{-1}	0.732
1.00	5.83×10^{-1}	7.08×10^{-1}	0.583

Figure 1 shows the acceleration profiles for a smooth pulse and a short pulse. At $\epsilon = 0.05$, the exact physical acceleration and the LL approximation are visually indistinguishable across the whole pulse. At $\epsilon = 0.50$, they separate: LL overshoots the peak and is displaced in time relative to the exact curve, and the shaded difference is a sizeable fraction of the signal. The departure is concentrated near the pulse peak, where $|\ddot{F}|$ is largest, as anticipated by hypothesis 2.

Figure 2 plots the two metrics against ϵ on logarithmic axes. For $\epsilon \lesssim 0.1$, both D_{rms} and D_{max} track the quadratic guide line of slope 2, confirming hypothesis 1. As ϵ approaches unity, the curves bend below slope 2. This is consistent with the decline of $D_{\mathrm{rms}}/\epsilon^2$ in Table 1: once the pulse is no longer slow on the scale τ_{e}, the single ϵ^2 term ceases to capture the full error and the comparison enters the regime where LL is not a controlled approximation.

The comparison also displays the time structure anticipated from the future-weighted integral. Both accelerations peak slightly before the force does, at $s < 0$, because the kernel in equation (5.3) samples the force ahead of the current instant. This is the pre-acceleration of Section 3 made visible.

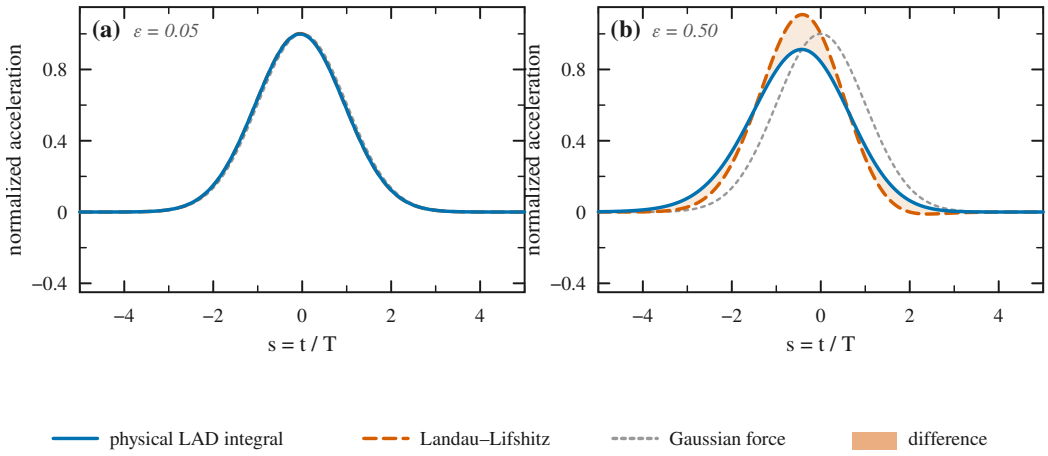

Figure 1. Normalized acceleration for a smooth pulse ($\epsilon = 0.05$, panel a) and a short pulse ($\epsilon = 0.50$, panel b). The exact physical LAD integral (5.3) (blue) is compared with the LL approximation (5.4) (vermillion) and the driving Gaussian force (grey). The shaded band marks their difference, which is negligible at $\epsilon = 0.05$ and pronounced at $\epsilon = 0.50$.

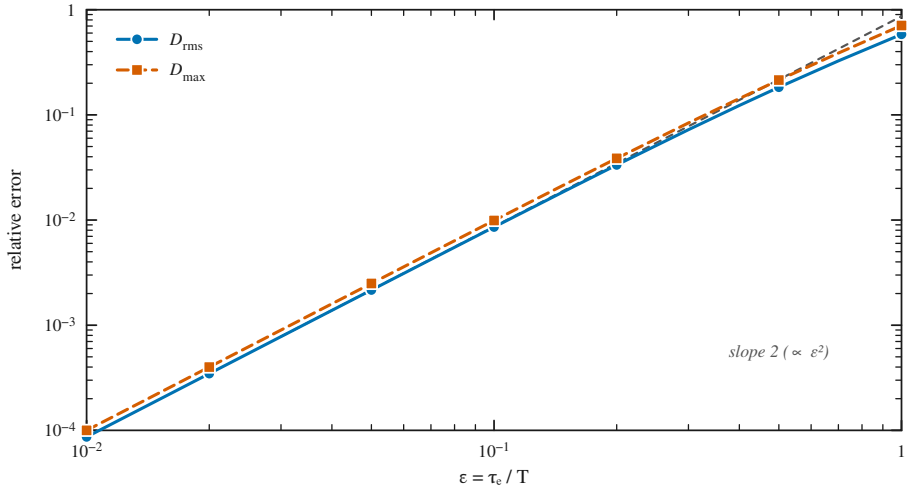

Figure 2. Relative error metrics D_{rms} (blue circles) and $D_{\max}$ (vermillion squares) versus $\epsilon = \tau_{\mathrm{e}}/T$ on log–log axes, with a slope-2 guide. The small-ϵ behaviour matches the predicted ϵ^2 scaling; the roll-off near $\epsilon \sim 1$ signals the breakdown of the first-order truncation.

The LL peak position is itself analytic: setting the derivative of equation (5.4) to zero gives

$$s_{\mathrm{peak}}^{\mathrm{LL}} = \frac{1 - \sqrt{1 + 4\epsilon^2}}{2\epsilon} \approx -\epsilon, \tag{5.6}$$

so the LL acceleration peaks a time of order ϵ (in units of T) ahead of the force. At $\epsilon = 0.5$ this evaluates to $s_{\mathrm{peak}}^{\mathrm{LL}} \approx -0.41$, in agreement with the tabulated value, and the exact peak sits a little earlier still. At small ϵ the exact and LL peaks coincide, but as ϵ grows the LL peak lags the exact

one: the positions stay within a grid spacing of each other up to $\epsilon \approx 0.3$ and then separate, reaching a displacement of order 0.08 in s at $\epsilon = 1$. The peak-height error and this peak displacement together account for the visible mismatch in Figure 1(b).

These results confirm all three hypotheses of Section 4.3: the error scales as ϵ^2 at small ϵ, it is largest near the pulse peak and grows toward $\epsilon \sim 1$, and it is independent of the field amplitude in the normalized linear model. The large-ϵ entries should be read as diagnostics of the approximation rather than descriptions of realistic pulses, since $\epsilon \sim 1$ would require a pulse duration comparable to $\tau_e \sim 6 \times 10^{-24}$ s.

The independence from amplitude is important because it connects the numerical section to the discussion of χ_e. If the pulse is multiplied by a constant factor, the profiles in Figure 1 grow by that same factor before normalization and the metrics in Table 1 are unchanged. Yet the same amplitude change would raise the rest-frame field and hence raise χ_e. The Gaussian benchmark therefore demonstrates, rather than merely asserts, that the classical LL–LAD error measured here is not a hidden quantum parameter in disguise. The field amplitude can make the classical model physically questionable without changing how well LL tracks the physical classical branch in this linear limit; this is why the regime map in the next section can display the computed error as vertical contours in the (ϵ, χ_e) plane.

5.4 Exact spectral error and its small-ϵ limit

Closed-form Gaussian accelerations have been used before to compare Abraham–Lorentz and LL motion [7]. Here the comparison is converted into an exact normalized error benchmark. Let $g(s) = e^{-s^2/2}$ and define $\widehat{h}(\omega) = \int_{\mathbb{R}} h(s) e^{-i\omega s}\, \mathrm{d}s$. The exact response A_ϵ and LL response L_ϵ obey

$$\widehat{A}_\epsilon(\omega) = \frac{\widehat{g}(\omega)}{1 - i\epsilon\omega}, \qquad \widehat{L}_\epsilon(\omega) = (1 + i\epsilon\omega)\widehat{g}(\omega), \tag{5.7}$$

and hence

$$\widehat{A}_\epsilon - \widehat{L}_\epsilon = -\frac{\epsilon^2\omega^2}{1 - i\epsilon\omega}\,\widehat{g}. \tag{5.8}$$

Parseval's identity and $|\widehat{g}|^2 \propto e^{-\omega^2}$ give the exact ratio

$$D^2_{\mathrm{rms}}(\epsilon) = \frac{\displaystyle\int_{-\infty}^{\infty} \frac{\epsilon^4\omega^4}{1 + \epsilon^2\omega^2} e^{-\omega^2}\, \mathrm{d}\omega}{\displaystyle\int_{-\infty}^{\infty} \frac{1}{1 + \epsilon^2\omega^2} e^{-\omega^2}\, \mathrm{d}\omega}. \tag{5.9}$$

Writing

$$J(\epsilon) = \int_{-\infty}^{\infty} \frac{e^{-\omega^2}}{1 + \epsilon^2\omega^2}\, \mathrm{d}\omega = \frac{\pi}{\epsilon} e^{1/\epsilon^2} \operatorname{erfc}\!\left(\frac{1}{\epsilon}\right), \tag{5.10}$$

polynomial division in the numerator of equation (5.9) yields

$$\boxed{D^2_{\mathrm{rms}}(\epsilon) = 1 - \frac{\sqrt{\pi}\,(1 - \epsilon^2/2)}{J(\epsilon)}} \qquad (\epsilon > 0). \tag{5.11}$$

Equation (5.11) is the principal analytic result of the benchmark. It covers the full scan, not only the perturbative region. At small ϵ, equation (5.9) or a scaled complementary error function is numerically preferable because the two terms in equation (5.11) nearly cancel.

The Gaussian moment expansion

$$J(\epsilon) = \sqrt{\pi}\left(1 - \frac{\epsilon^2}{2} + \frac{3\epsilon^4}{4} - \frac{15\epsilon^6}{8} + O(\epsilon^8)\right) \tag{5.12}$$

then gives

$$D_{\mathrm{rms}} = \frac{\sqrt{3}}{2}\epsilon^2\left[1 - \epsilon^2 + 3\epsilon^4 + O(\epsilon^6)\right]. \tag{5.13}$$

The leading time-domain error is $\epsilon^2 g''(s)$, so $D_{\max}/\epsilon^2 \to 1$. The dependency-free script evaluates equation (5.9) separately in frequency space. Across the reported scan it agrees with direct evaluation of the future integral to the tolerance recorded in Simulations/data/summary.json. This checks the full norm identity, while the approach to $\sqrt{3}/2$ checks the asymptotic coefficient.

With ϵ established as the parameter that governs the classical reduction-of-order error, the remaining question is how this criterion sits beside the quantum parameter χ_{e}, which is the subject of Section 6.

6 Relation to χ_{e}

6.1 A different small parameter

The preceding benchmark answers a classical approximation question. Strong-field experiments also ask whether a deterministic classical emission model is adequate in the first place. The electron quantum parameter is

$$\chi_{\mathrm{e}} = \frac{e\hbar}{m^3c^4}\sqrt{-(F^{\mu\nu}p_\nu)^2} \simeq \frac{\gamma E_{\mathrm{eff}}}{E_{\mathrm{S}}}, \qquad E_{\mathrm{S}} = \frac{m^2c^3}{e\hbar} \approx 1.3\times10^{18}\ \mathrm{V\,m^{-1}}. \tag{6.1}$$

It measures the field in the electron rest frame relative to the Schwinger scale and controls the importance of recoil and quantum corrections to emission [4, 15]. Some experimental papers denote the same parameter by η; we use χ_{e} throughout.

The two parameters answer different questions. Here $\epsilon = \tau_{\mathrm{e}}/T$ measures the error made by truncating the non-runaway classical response, whereas χ_{e} concerns the physical adequacy of a classical emission model. In the normalized linear benchmark they are independent by construction: changing T changes ϵ, while multiplying the prescribed field changes χ_{e} but cancels from D_{rms} and $D_{\max}$. This factorization is not universal. In a relativistic laser collision the field variation experienced by the electron depends on its trajectory and Doppler-shifted laser phase, so duration, amplitude, and energy no longer separate cleanly [8, 11].

Quantum corrections can already be measurable around $\chi_{\mathrm{e}} \sim 0.1$; $\chi_{\mathrm{e}} \sim 1$ is a stronger guide for order-unity recoil and pronounced stochasticity. The recent experiment of Los et al. reported evidence favouring quantum-continuous and quantum-stochastic models over a classical model for mean quantum parameter roughly 0.05–0.1, not for $\chi_{\mathrm{e}} > 1$ [14]. Earlier collision experiments also probed the onset of radiation-reaction and quantum-emission effects [12, 13]. These observations motivate the vertical scale used below, but they are not tests of the present nonrelativistic Gaussian formula.

6.2 Diagnostic map

Figure 3 places the two diagnostics on separate axes. The colour field and vertical contours are not fitted experimental data: they encode the exact Gaussian value $D_{\mathrm{rms}}(\epsilon)$ from equation (5.11). The horizontal lines are interpretive guides at $\chi_{\mathrm{e}} = 0.1$ and 1.

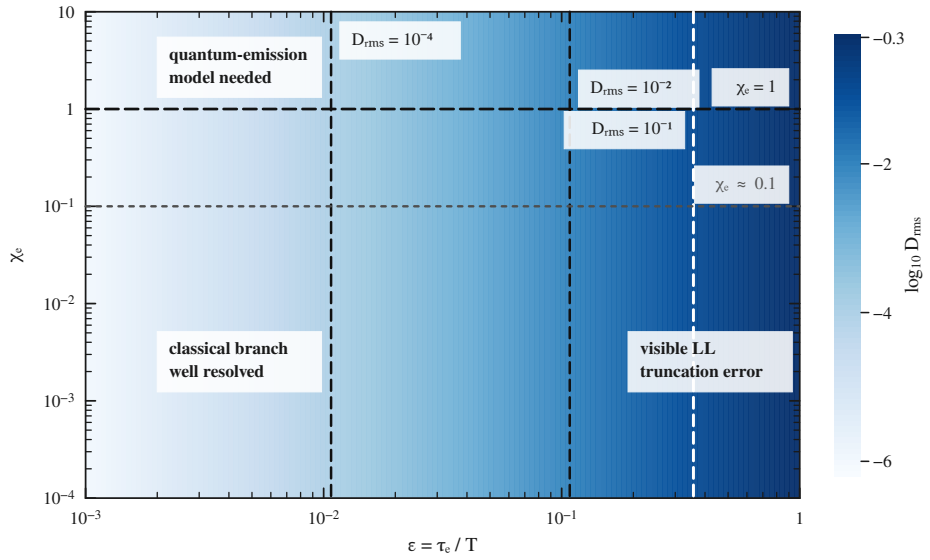

Figure 3. Diagnostic map in the $(\epsilon, \chi_{\mathrm{e}})$ plane. Colour and vertical contours show the exact Gaussian reduction-of-order error $D_{\mathrm{rms}}(\epsilon)$, independent of χ_{e} only within the normalized linear model. Horizontal guides mark the onset of appreciable quantum corrections near $\chi_{\mathrm{e}} \sim 0.1$ and the strong-recoil scale $\chi_{\mathrm{e}} \sim 1$.

The map prevents a category error. Moving horizontally changes how accurately LL approximates the selected classical branch in this model. Moving vertically changes whether a classical emission picture is adequate. A large value on one axis does not logically imply a large value on the other, even though realistic relativistic configurations can correlate them.

6.3 Laboratory scale and scope

For a femtosecond-scale envelope,

$$\epsilon = \frac{\tau_{\mathrm{e}}}{T} \lesssim 10^{-8}, \tag{6.2}$$

so equation (5.13) puts the particular truncation error studied here below order 10^{-16}. This does not prove that every LL-based laser calculation is accurate: spatial gradients, relativistic motion, radiation dominance, pulse structure, and numerical modelling are absent. It shows only that the envelope timescale by itself cannot produce a measurable LL–Abraham–Lorentz discrepancy in this benchmark.

A relativistic continuation would replace the prescribed force by the force sampled along the particle trajectory and compare the LL solution with a carefully selected LAD branch. Exact LL plane-wave solutions and relativistic LAD–LL comparisons show that this problem is considerably

richer [8, 11]. The useful quantity to retain is the normalized error norm; the clean separation into independent ϵ and χ_e axes should not be assumed to survive.

7 Limitations and conclusion

7.1 Limitations

The benchmark is deliberately narrow, and its limits should be stated plainly. The model is nonrelativistic, one-dimensional, and driven by an externally prescribed field. It captures the reduction-of-order structure, but not the geometry of a real laser–electron collision, where the field depends on position, the magnetic force matters, and the electron is relativistic. The field is treated as a fixed background; back-reaction on the field and collective effects are absent by construction.

A second limitation is dimensional. Because $\tau_e \sim 6 \times 10^{-24}$ s is so small, a pulse with T comparable to τ_e is far outside any realistic laboratory regime, and at such scales the point-particle classical model is itself questionable. The large-ϵ entries in Section 5 are therefore diagnostics of the approximation, chosen to expose the scaling, not predictions for an experiment. Finally, the paper makes no attempt at a relativistic LAD integration, an exact plane-wave treatment, or a stochastic quantum-emission calculation. The strong-field discussion of Section 6 is interpretive, and the quantitative claims are confined to the classical toy model.

A further caveat concerns the point-particle idealization. The Abraham–Lorentz model gives the electron no internal structure, uses a future boundary condition to remove the runaway mode, and omits spin. These are serious limitations if the result is interpreted as a literal electron trajectory, but they do not change the benchmark's purpose: testing the local LL truncation against an exactly specified non-runaway branch.

The simplicity of the benchmark also means that it should not be used to rank competing radiation-reaction models in realistic simulations. In the present calculation the external force is prescribed, so the electron trajectory does not feed back into the force it samples. A real laser pulse changes along the particle path, and the particle path changes because of radiation reaction. That feedback is where the relativistic LL equation earns its usefulness and where a direct comparison with LAD becomes technically difficult. The present result is therefore best read as a calibration calculation: it fixes the meaning of "LL approximates the physical LAD branch" in a case where the answer is unambiguous, and it supplies a small parameter that can be looked for, in modified form, in more complicated problems.

There is also a limitation in the way the quantum discussion is framed. The parameter χ_e is a powerful diagnostic, but it is not a complete theory of strong-field emission. It summarizes the typical recoil scale and helps decide when quantum spectra and stochastic emission matter, yet detailed predictions require an emission model, particle distribution, laser geometry, and detector response. The two-axis map in Section 6 should therefore be understood as a conceptual classification, not as a replacement for a full strong-field QED or Monte Carlo calculation. Its value is to prevent a category error: using χ_e to diagnose the quantum validity of the classical picture should not be confused with diagnosing the mathematical accuracy of the LL reduction of order.

7.2 Conclusion

In the nonrelativistic one-dimensional Abraham–Lorentz limit, τ_e multiplies the highest derivative, so $\tau_e \to 0$ is a singular limit rather than a regular deletion of a small force. Selecting the non-runaway branch first gives a future-weighted integral; LL is its first local derivative truncation. For a Gaussian pulse, Parseval's identity gives the exact finite-ϵ error in equation (5.11), and its expansion begins $D_{\mathrm{rms}} = (\sqrt{3}/2)\epsilon^2(1 - \epsilon^2 + 3\epsilon^4 + \cdots)$. Independent time-domain quadrature reproduces that curve. This answers the mathematical part of the research question without integrating the unstable runaway equation as an initial-value problem.

The second half concerns χ_e. It asks not whether LL approximates the selected classical branch, but whether a classical emission model is physically adequate. In the linear benchmark the amplitude sets χ_e but cancels from the normalized LL–Abraham–Lorentz error. The map in Section 6 displays that logical separation while explicitly limiting it to the prescribed-force model.

For a femtosecond-scale envelope, ϵ is at most of order 10^{-8}, so the truncation error isolated by this benchmark is negligible. This statement does not establish the accuracy of LL in every relativistic geometry; it only removes one proposed explanation in the present limit. Conversely, an artificial short-pulse benchmark can make LL visibly inaccurate while χ_e remains small, showing why a stochastic quantum model would answer a different question.

The practical use is simulation hygiene. Strong-field calculations distinguish deterministic radiation-reaction forces from quantum-corrected or stochastic emission modules [15, 16]. The Gaussian benchmark cannot predict those systems, but it supplies a portable diagnostic question: is a discrepancy caused by reduction of order, by failure of the classical emission picture, or by modelling outside either description?

Against existing Abraham–Lorentz/LL comparisons, the contribution is not the Gaussian solution alone. It is the exact normalized L^2 error formula, its controlled asymptotics, the reproducible cross-check, and the diagnostic separation of ϵ from χ_e.

A Gaussian moment integrals for the error coefficients

The leading and next-to-leading coefficients quoted in Section 5.4 follow from a compact set of Gaussian integrals, collected here for completeness. Writing $g(s) = e^{-s^2/2}$, the derivatives that enter the error are

$$g' = -s\,g, \qquad g'' = (s^2 - 1)\,g, \qquad g''' = s(3 - s^2)\,g, \qquad g'''' = (s^4 - 6s^2 + 3)\,g. \tag{A.1}$$

Every integral needed reduces to the standard even Gaussian moments

$$\int_{-\infty}^{\infty} s^{2k} e^{-s^2}\,\mathrm{d}s = \frac{(2k-1)!!}{2^k}\sqrt{\pi}, \tag{A.2}$$

giving $\int e^{-s^2} = \sqrt{\pi}$, $\int s^2 e^{-s^2} = \frac{1}{2}\sqrt{\pi}$, $\int s^4 e^{-s^2} = \frac{3}{4}\sqrt{\pi}$, and $\int s^6 e^{-s^2} = \frac{15}{8}\sqrt{\pi}$. Substituting the squares of equation (A.1),

$$\int g^2 = \sqrt{\pi}, \qquad \int g'^2 = \frac{\sqrt{\pi}}{2}, \qquad \int g''^2 = \frac{3\sqrt{\pi}}{4}, \qquad \int g'''^2 = \frac{15\sqrt{\pi}}{8}, \tag{A.3}$$

where all integrals run over the real line.

The closed form in equation (5.10) follows without a table of integrals. For real x,

$$\frac{1}{1+x^2} = \int_0^\infty e^{-t}\cos(xt)\,\mathrm{d}t. \tag{A.4}$$

Substitution into $J(\epsilon)$, followed by the Gaussian Fourier integral, gives

$$J(\epsilon) = \sqrt{\pi}\int_0^\infty e^{-t-\epsilon^2 t^2/4}\,\mathrm{d}t \tag{A.5}$$

$$= \frac{\pi}{\epsilon}e^{1/\epsilon^2}\operatorname{erfc}\left(\frac{1}{\epsilon}\right). \tag{A.6}$$

This also makes positivity of J immediate and supplies the large-$1/\epsilon$ expansion used below.

At leading order in ϵ the normalized error is $\epsilon^2 g''$ and the denominators in equation (5.5) reduce to $\int g^2$, so

$$\left.\frac{D_{\mathrm{rms}}}{\epsilon^2}\right|_{\epsilon\to 0} = \left(\frac{\int g''^2}{\int g^2}\right)^{1/2} = \sqrt{\tfrac{3}{4}} = \frac{\sqrt{3}}{2}, \qquad \left.\frac{D_{\max}}{\epsilon^2}\right|_{\epsilon\to 0} = \frac{|g''(0)|}{g(0)} = 1, \tag{A.7}$$

since $|g''|$ attains its maximum value 1 at $s = 0$, where $g = 1$. For the next order, the numerator and denominator of D_{rms}^2 pick up the first corrections from the higher terms of the series (4.3); using $\int g''g'''' = -\int g'''^2$ (integration by parts), with the odd cross terms vanishing by parity,

$$N = \epsilon^4\int g''^2 - \epsilon^6\int g'''^2 + \cdots, \qquad D = \int g^2 - \epsilon^2\int g'^2 + \cdots. \tag{A.8}$$

Forming the ratio and expanding,

$$\frac{D_{\mathrm{rms}}^2}{\epsilon^4} = \frac{\int g''^2}{\int g^2}\left(1-\epsilon^2\frac{\int g'''^2}{\int g''^2}\right)\left(1-\epsilon^2\frac{\int g'^2}{\int g^2}\right)^{-1} + \cdots = \frac{3}{4}\left(1-2\epsilon^2\right) + \cdots, \tag{A.9}$$

where $\int g'''^2/\int g''^2 = \frac{5}{2}$ and $\int g'^2/\int g^2 = \frac{1}{2}$. Taking the square root gives equation (5.13), $D_{\mathrm{rms}}/\epsilon^2 = (\sqrt{3}/2)(1-\epsilon^2+\cdots)$, which is the curve compared with Table 1 in Section 5.4.

B Dimensionless form of the benchmark

The dimensionless expressions (5.3) and (5.4) follow from the closed forms of Section 3 by direct substitution. For the Gaussian pulse the force is $F(t) = -F_0\,e^{-t^2/2T^2}$ with $F_0 = eE_0$, and with $s = t/T$ and $\epsilon = \tau_{\mathrm{e}}/T$ the shifted argument in equation (3.4) becomes $t + \tau_{\mathrm{e}}u = T(s+\epsilon u)$. Hence

$$a_{\mathrm{LAD}}(t) = \frac{1}{m}\int_0^\infty e^{-u}F(t+\tau_{\mathrm{e}}u)\,\mathrm{d}u = -\frac{F_0}{m}\int_0^\infty e^{-u}\exp\left[-\frac{(s+\epsilon u)^2}{2}\right]\mathrm{d}u, \tag{B.1}$$

and dividing by $-F_0/m$ (absorbing the overall sign as in Section 5.1) reproduces equation (5.3). For the LL acceleration, $\dot F = -F_0(\mathrm{d}/\mathrm{d}t)e^{-t^2/2T^2} = (F_0 s/T)e^{-s^2/2}$, so

$$a_{\mathrm{LL}}(t) = \frac{1}{m}\left[F + \tau_{\mathrm{e}}\dot F\right] = -\frac{F_0}{m}\,e^{-s^2/2}\,(1-\epsilon s)\,, \tag{B.2}$$

which on dividing by $-F_0/m$ gives equation (5.4). The factor $1-\epsilon s$ is the origin of the time displacement of the LL peak discussed in Section 5.3.

Acknowledgments

This work began as a PHY204 Electrodynamics I term paper at Xiamen University Malaysia. Both authors approved the present revision and its public release.

Data and code availability: the complete source, simulation code, generated data, and figure files are available at github.com/hhungxun/physics-writeups. Running Simulations/scripts/run_gaussian_benchmark.py reproduces Table 1 and Figures 1–3.

AI disclosure: generative-AI tools assisted with language editing, code scaffolding, and adversarial checks during revision. The authors checked the retained derivations, citations, code, and prose and take responsibility for the manuscript.

References

[1] P.A.M. Dirac, *Classical theory of radiating electrons*, Proc. Roy. Soc. Lond. A **167** (1938) 148, doi:10.1098/rspa.1938.0124.

[2] L.D. Landau and E.M. Lifshitz, *The Classical Theory of Fields*, Course of Theoretical Physics, Vol. 2, 4th ed., Pergamon Press, Oxford (1975).

[3] H. Spohn, *The critical manifold of the Lorentz–Dirac equation*, Europhys. Lett. **50** (2000) 287, arXiv:physics/9911027.

[4] A. Di Piazza, C. Muller, K.Z. Hatsagortsyan and C.H. Keitel, *Extremely high-intensity laser interactions with fundamental quantum systems*, Rev. Mod. Phys. **84** (2012) 1177, doi:10.1103/RevModPhys.84.1177.

[5] D.A. Burton and A. Noble, *Aspects of electromagnetic radiation reaction in strong fields*, Contemp. Phys. **55** (2014) 110, doi:10.1080/00107514.2014.886840.

[6] D.J. Griffiths, T.C. Proctor and D.F. Schroeter, *Abraham–Lorentz versus Landau–Lifshitz*, Am. J. Phys. **78** (2010) 391, doi:10.1119/1.3269900.

[7] A. Shaw, *Elimination of pathological solutions of the Abraham–Lorentz equation of motion*, arXiv:2205.14809.

[8] A. Di Piazza, *Exact solution of the Landau–Lifshitz equation in a plane wave*, Lett. Math. Phys. **83** (2008) 305, arXiv:0801.1751.

[9] R. Ekman, T. Heinzl and A. Ilderton, *Reduction of order, resummation and radiation reaction*, Phys. Rev. D **104** (2021) 036002, doi:10.1103/PhysRevD.104.036002.

[10] R. Ekman, *Reduction of order and transseries structure of radiation reaction*, Phys. Rev. D **105** (2022) 056016, doi:10.1103/PhysRevD.105.056016.

[11] A.D. Yaghjian, *Lorentz–Abraham–Dirac and Landau–Lifshitz equations of motion and the solution to a relativistic electron in a counterpropagating laser beam*, Phys. Rev. Accel. Beams **24** (2021) 114002, doi:10.1103/PhysRevAccelBeams.24.114002.

[12] J.M. Cole et al., *Experimental evidence of radiation reaction in the collision of a high-intensity laser pulse with a laser-wakefield accelerated electron beam*, Phys. Rev. X **8** (2018) 011020, doi:10.1103/PhysRevX.8.011020.

[13] K. Poder et al., *Experimental signatures of the quantum nature of radiation reaction in the field of an ultra-intense laser*, Phys. Rev. X **8** (2018) 031004, doi:10.1103/PhysRevX.8.031004.

[14] E.E. Los et al., *Observation of quantum effects on radiation reaction in strong fields*, Nature Commun. **17** (2026) 1157, doi:10.1038/s41467-025-67918-8.

[15] T.G. Blackburn, *Radiation reaction in electron–beam interactions with high-intensity lasers*, Rev. Mod. Plasma Phys. **4** (2020) 5, doi:10.1007/s41614-020-0042-0.

[16] C.P. Ridgers, J.G. Kirk, R. Duclous, T. Blackburn, C.S. Brady, K. Bennett, T.D. Arber and A.R. Bell, *Modelling gamma-ray photon emission and pair production in high-intensity laser–matter interactions*, J. Comput. Phys. **260** (2014) 273, doi:10.1016/j.jcp.2013.12.007.

[17] P.O. Kazinski and M.A. Shipulya, *Asymptotics of physical solutions to the Lorentz–Dirac equation for a planar motion in constant electromagnetic fields*, Phys. Rev. E **83** (2011) 066606, arXiv:1012.5728.